THE JOURNAL OF BIOLOGICAL CHEMISTRY
Vol. 279, No. 29, Issue of July 16, pp. 30781–30790, 2004

Printed in U.S.A.

Crystallographic and Biophysical Analysis of a Bacterial Signal Peptidase in Complex with a Lipopeptide-based Inhibitor*

Received for publication, February 16, 2004, and in revised form, April 27, 2004
Published, JBC Papers in Press, May 10, 2004, DOI 10.1074/jbc.M401686200

Mark Paetzel‡§, Jonathon J. Goodall¶, Malgosia Kania¶, Ross E. Dalbey‖, and Malcolm G. P. Page¶

From the ‡Department of Molecular Biology and Biochemistry, Simon Fraser University, Burnaby, British Columbia, V5A 1S6 Canada, ¶Basilea Pharmaceutica Ltd., Grenzacherstrasse 487, CH-4058, Basel, Switzerland, and the ‖Department of Chemistry, The Ohio State University, Columbus, Ohio 43210

We report here the crystallographic and biophysical analysis of a soluble, catalytically active fragment of the *Escherichia coli* type I signal peptidase (SPase Δ2–75) in complex with arylomycin A_2. The 2.5-Å resolution structure revealed that the inhibitor is positioned with its COOH-terminal carboxylate oxygen (O45) within hydrogen bonding distance of all the functional groups in the catalytic center of the enzyme (Ser^{90} O-γ, Lys^{145} N-ζ, and Ser^{88} O-γ) and that it makes β-sheet type interactions with the β-strands that line each side of the binding site. Ligand binding studies, calorimetry, fluorescence spectroscopy, and stopped-flow kinetics were also used to analyze the binding mode of this unique non-covalently bound inhibitor. The crystal structure was solved in the space group $P4_32_12$. A detailed comparison is made to the previously published acyl-enzyme inhibitor complex structure (space group: $P2_12_12$) and the apo-enzyme structure (space group: $P4_12_12$). Together this work provides insights into the binding of pre-protein substrates to signal peptidase and will prove helpful in the development of novel antibiotics.

Type I signal (leader) peptidase (SPase,[1] EC 3.4.21.89) is the membrane-bound serine endopeptidase that catalyzes the cleavage of the amino-terminal signal (or leader) peptide from secretory proteins and some membrane proteins (for recent reviews, see Refs. 1–3). Evolutionarily, SPase belongs to the protease clan SF and the protease family S26 (4). The *Escherichia coli* SPase has served as the model Gram-negative SPase and is the most thoroughly characterized SPase to date. It has been cloned (5), sequenced (6), overexpressed (7), purified (6, 8, 9), and kinetically (10), and structurally (11, 12) characterized. *E. coli* SPase (323 amino acids, 35,988 Da, pI 6.9) contains two amino-terminal transmembrane segments (residues 4–28 and 58–76), a small cytoplasmic region (residues 29–58), and a carboxyl-terminal periplasmic catalytic region (residues 77–323). A catalytically active fragment of SPase (SPase Δ2–75) corresponding to the periplasmic region (lacking the two transmembrane segments and the cytoplasmic domain) has been cloned, purified, characterized (13, 14), and crystallized (15). Interestingly, the Δ2–75 construct required detergent or lipid for optimal activity (14) and crystallization (15).

The crystal structure of Δ2–75 has been solved in complex with a β-lactam-type inhibitor as well in the apo-form (11, 12). The structures of *E. coli* SPase Δ2–75 revealed that the periplasmic region of bacterial signal peptidase has a unique, mostly β-structure protein fold made of several coiled β-sheets and contains an Src homology 3-like barrel. The periplasmic region of SPase is made up of two domains. Domain I contains the catalytic residues and all of the conserved regions of sequence. It also contains an unusually large exposed hydrophobic surface that is consistent with a membrane association surface and possibly the detergent/lipid requirement of the Δ2–75 deletion construct. The second β-sheet domain, domain II, is an insertion within domain I and appears to be mostly present in Gram-negative signal peptidases (16).

Site-directed mutagenesis (10, 17), chemical modification (10, 18), and crystallographic (11, 12) studies are consistent with SPase utilizing a Ser-Lys dyad mechanism whereby Ser^{90} serves as the nucleophile and Lys^{145} serves as the general base. Kinetic analysis of site-directed mutants designed using the crystal structure (11) has revealed that *E. coli* SPase contains an unusual oxyanion hole that uses hydrogen bonds from a serine hydroxyl hydrogen (Ser^{88} O-γH) and a main chain amide hydrogen (Ser^{90} NH) to stabilize the transition state oxyanion at the scissile bond (19). The crystal structures with and without covalently bound inhibitor have helped to explain the Ala-*X*-Ala substrate specificity by revealing two shallow hydrophobic pockets (S1 and S3) adjacent to the catalytic residues and leading to the proposed membrane association surface (11, 12). The structures also reveal that SPase is an unusual serine protease in that it attacks the scissile amide bond of the substrate from the *si*-face rather than the *re*-face, as seen in most serine proteases (20, 21).

It has been observed in many laboratories that bacterial type I SPases are not inhibited by standard protease inhibitors (13, 22–24). The first effective synthetic signal peptidase inhibitors to be discovered were described by Kuo and collegues in 1994 (25). They showed that β-lactam analogs inhibited *E. coli* SPase. The most effective β-lactam (penem) compounds are the

* This work was supported in part by a Canadian Institute of Health Research operating grant (to M. P.), the Michael Smith Foundation for Health Research, a National Science and Engineering Research Council of Canada operating grant (to M. P.), and National Science Foundation Grant MCB-0316670 (to R. E. D.). The costs of publication of this article were defrayed in part by the payment of page charges. This article must therefore be hereby marked "*advertisement*" in accordance with 18 U.S.C. Section 1734 solely to indicate this fact.

The atomic coordinates and structure factors (code 1T7D) have been deposited in the Protein Data Bank, Research Collaboratory for Structural Bioinformatics, Rutgers University, New Brunswick, NJ (http://www.rcsb.org/).

§ Michael Smith Foundation for Health Research scholar award recipient. To whom correspondence should be addressed: Dept. of Molecular Biology and Biochemistry, Simon Fraser University, South Science Bldg., 8888 University Dr., Burnaby, British Columbia, V5A 1S6 Canada. Tel.: 604-291-4230, (Lab) 604-291-4318; Fax: 604-291-5583; E-mail: mpaetzel@sfu.ca.

[1] The abbreviations used are: SPase, signal peptidase; Δ2–75, the construct of *E. coli* signal peptidase lacking residues 2 through 75, which correspond to the transmembrane segments and the cytoplasmic region; MeHpg, *N*-methyl-4-hydroxyphenylglycine.

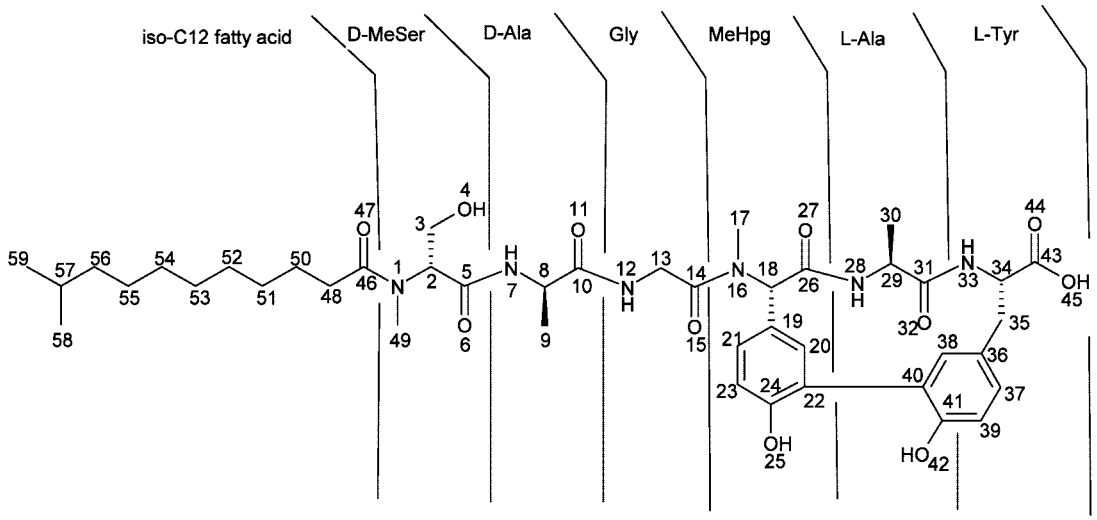

FIG. 1. **Structure of the signal peptidase inhibitor/antibiotic arylomycin A_2.** All non-hydrogen inhibitor atoms are numbered. MeHpg is *N*-methyl-4-hydroxyphenylglycine.

5 S stereoisomers (26). A crystal structure of *E. coli* SPase Δ2–75 has been solved with the compound allyl (5*S*,6*S*)-6-((*R*)-acetoxyethyl)-penem-3-carboxylate covalently bound to the nucleophilic Ser^{90} O-γ (11). It has also been previously observed that *E. coli* SPase can be competitively inhibited by signal peptides or by pre-proteins with proline at the P1′ (+1) position (27, 28).

Arylomycin A_2 is a member of a recently described class of antibiotics (29) that have been shown to be inhibitors of SPase.[2] Arylomycins are lipohexapeptides (D-MeSer–D-Ala–Gly–L-MeHpg–L-Ala–L-Tyr) with a 12-carbon atom branched fatty acid (isoC12) attached via an amide bond to the amino terminus (Fig. 1). The amino acid residue MeHpg is *N*-methyl-4-hydroxyphenylglycine. Interestingly, the MeHpg is cross-linked via the ortho-carbon atom of its phenol ring to the ortho-carbon atom in the phenol ring of the Tyr residue forming a (3,3)-biaryl bridge. This cross-link creates a 3-residue ring-type structure within the peptide. Two of the backbone amide nitrogen atoms (MeSerN1 and MeHpgN16) are methylated. The first two residues have D-stereochemistry. The crystallographic and biophysical analysis of the mode of binding of this inhibitor in the substrate binding cleft of *E. coli* signal peptidase reveals the mechanism of inhibition for this non-covalently bound peptide-based inhibitor and also may give us important insights into the binding interactions involved in pre-protein binding and cleavage by type I signal peptidase.

EXPERIMENTAL PROCEDURES

Materials—The SPase Δ2–75 protein (relative molecular mass (M_r) 27,952 by electrospray ionization mass spectrometry analysis (13) (249 amino acid residues, measured isoelectric point of 5.6 (15)) was expressed and purified as described previously (15). The Δ2–75 protein (10 mg/ml) was suspended in 20 mM Tris-HCl, pH 7.4, and 0.5% Triton X-100. The inhibitor arylomycin A_2 was isolated from *Streptomyces* as described by Schimana *et al.* (29).

Co-crystallization and Data Collection—Arylomycin A_2, dissolved in Me_2SO and water, was added to the SPase Δ2–75 protein at a 1:1 mole ratio and allowed to sit on ice for >30 min and then stored at −20 °C. The crystals were grown by sitting drop vapor diffusion with a reservoir consisting of 0.5% Triton X-100, 15% PEG 4000, 20% propanol-1, and 0.1 M sodium citrate, pH 6.0. The drop consisted of 1 μl of the protein-inhibitor mixture and 1 μl of the reservoir solution. The crystals belong to the tetragonal space group $P4_32_12$ with unit cell dimensions of a = 69.6 Å, b = 69.6 Å, c = 258.5 Å. Given the unit cell dimensions and the molecular mass, the specific volume (V_m (30)) is 2.8 $Å^3$/Da for two molecules in the asymmetric unit. Before data collection, the crystal was soaked in a cryosolution that consisted of the same conditions as the crystallization mother liquor with the addition of 20% glycerol. The x-ray diffraction intensities were measured at 100 K on beamline X8C at the Brookhaven National Laboratory, National Synchrotron Light Source (NSLS). The data were processed using DENZO and SCALEPACK (31). See Table I for data collection statistics.

Phasing, Model Building, and Refinement—A molecular replacement solution was found using the program AmoRe (32). Molecule A from the previously published inhibitor acyl-enzyme crystal structure of *E. coli* SPase Δ2–75 was used as a search model (Ref. 11; Protein Data Bank code 1b12). Model building and analysis was performed with the program XFIT within the suite XTALVIEW (33). Refinement of the structure was carried out using the program CNS (34). The topology and parameter files for the lipohexapeptide inhibitor were generated using the programs XPLO2D (35) and PRODRG (36). The stereochemistry of the molecular models was analyzed with the programs PROCHECK (37).

Structural Analysis—The secondary structural analysis was performed with the program PROMOTIF (38). The utilities Lsq_explicit, Lsq_improve, and Lsq_molecule within the program O (39) were used to superimpose the Δ2–75 molecules for comparing the different molecules in the asymmetric unit or for comparing molecules from different structures. The program CONTACT within the program suite CCP4 (32) was used to measure the hydrogen bond and van der Waals contacts between the inhibitor and the enzyme. The program CAST (40) was used to measure the S1 and S3 binding sites. The program SURFACE RACER 1.2 (41) was used to measure the solvent accessible surface. A probe radius of 1.4 Å was used in the calculations.

Figure Preparation—Fig. 1 was prepared using the program ISIS Draw version 2.1.4 (MDL Information Systems, Inc.). Fig. 2 was prepared using the programs XFIT (33) and Raster3D (42). Figs. 3 and 4 were prepared using the programs Molscript (43) and Raster3D (42).

Accession Numbers—Atomic coordinates for the SPase Δ2–75 peptide-based inhibitor (arylomycin A_2) complex structure have been deposited with the RCSB Protein Data Bank (44) under accession code 1T7D. Atomic coordinates for the SPase Δ2–75 β-lactam-type inhibitor acyl-enzyme complex structure (11) are under accession code 1B12 and the SPase Δ2–75 apo-enzyme structure (12) is under accession code 1KN9.

Fluorescence Spectroscopy of Ligand Binding—Steady-state fluorescence measurements were made using a PerkinElmer LS-50 spectrofluorimeter. Spectra were recorded between 250 and 300 nm for excitation and between 310 and 450 nm for emission. The protein concentration was between 1 and 10 mM and ligand was in excess. Both enzyme and ligand were in 20 mM Tris-HCl, pH 7.4, 5 mM $MgCl_2$, 1% Elugent™ detergent and all experiments were carried out at 25 °C.

Stopped-flow Experiments under Conditions of Excess Substrate—The kinetics of arylomycin A_2 binding to SPase were investigated by stopped-flow fluorescence and stopped-flow fluorescence anisotropy on a model SF-61 DX2 stopped-flow spectrometer from Hi-Tech. The excitation wavelengths in each case were set using a monochromator and the fluorescence emission was measured using a filter with a cut-off

[2] M. G. P. Page, manuscript in preparation.

TABLE I
Crystallographic data

$R_{merge} = \Sigma ||I_{o,i}|-|I_{ave,i}||/ \Sigma |I_{ave,i}|$, where $I_{ave,i}$ is the average structure factor amplitude of reflection I , and $I_{o,i}$ represents the individual measurements of reflection I and its symmetry equivalent reflection. $R = \Sigma | F_o - F_c|/\Sigma F_o$ (on all data, 40.0–2.47 Å). $R_{free} = \Sigma_{hkl\delta T}(|F_o|-|F_c|)^2/\Sigma_{hkl\delta T}|F_o|^2$, where $\Sigma_{hkl\delta T}$ are reflections belonging to a test set of 10% of the data, and F_o and F_c are the observed and calculated structure factors, respectively. The data collection statistics in parentheses are the values for the highest resolution shell (2.56–2.47 Å).

Data collection	
Space group	$P4_32_12$
Unit cell dimensions (Å)	69.6 × 69.6 × 258.5
Molecules in assymetric units	2
V_m (Å^3/Da)	2.8
Resolution (Å)	40.0–2.47
Total observed reflections	115,418
Unique reflections	21,656
% possible	90.9 (86.4)
$I/\sigma(I)$	19.4 (8.0)
R_{merge} (%)	7.7 (18.3)
Refinement	
Residues	431
Protein atoms	3403
Waters	272
R	23.1
R_{free}	28.5
Root mean square deviations	
Bonds (Å)	0.0073
Angles (°)	1.4199
Average overall B (Å^2) (protein and water)	50.8
Average inhibitor B (Å^2)	53.6

below 360 nm. For stopped-flow fluorescence measurements the excitation wavelength was set at 280 nm to excite the arylomycin A_2 molecule through the tryptophans of the SPase enzyme, whereas for anisotropy measurements the excitation wavelength was set at 310 nm to excite the ligand directly. In all cases the stopped-flow fluorescence data used for analysis were the average of 5 kinetic runs obtained under the exact same conditions and concentrations.

The rate of binding was measured under conditions of excess substrate, with the SPase concentration kept at 6.25 μM and the ligand concentration varied in the range 7.5–50 μM and under conditions of excess enzyme with the enzyme concentration again at 6.25 μM and the ligand concentration varied in the concentration range 0.05–5 μM. Both enzyme and ligand were in 20 mM Tris-HCl, pH 7.4, 5 mM $MgCl_2$, 1% Elugent™ detergent and all experiments were carried out at 25 °C. Stopped-flow data were fitted to a double exponential equation of the form,

$$\Delta F = \Delta F_1 \times (1 - \exp^{(k_1 \times t)}) + \Delta F_2 \times (1 - \exp^{(-k_2 \times t)}) + c \qquad \text{(Eq. 1)}$$

where ΔF is the total change in fluorescence, ΔF_1 and ΔF_2 are the fluorescence changes associated with rate constants k_1 and k_2, k_1 and k_2 are first-order rate constants, and c is the offset.

The observed rate of binding under conditions of excess substrate was then plotted against the ligand concentration and fitted to Equation 2,

$$k_{obs} = k_{off} + k_{on} \cdot [L] \qquad \text{(Eq. 2)}$$

where k_{obs} (s^{-1}) is the observed first-order rate of binding, k_{off} (s^{-1}) is the first-order rate constant for dissociation, k_{on} ($M^{-1}\,s^{-1}$) is the second-order rate constant for association (28), and M is the concentration of free ligand.

Differential Scanning Calorimetry—The thermal stability of signal peptidase under various conditions was investigated by differential scanning calorimetry using a Microcal VP-DSC (Microcal Inc.) microcalorimeter. Solutions of 12.5 μM SPase in 20 mM Hepes-NaOH, 1% Elugent™ detergent, with and without 100 μM arylomycin A_2 were used as samples. All solutions were thoroughly degassed before use and the reference cell in each case was filled with an aliquot of buffer against which the protein solution had previously been dialyzed overnight. All samples were scanned from 30 to 70 °C, at a rate of 1 °C/min and data were baseline corrected, smoothed using a Savitsky-Golay 9 point smoothing algorithm, and analyzed using the Origin Scientific plotting software.

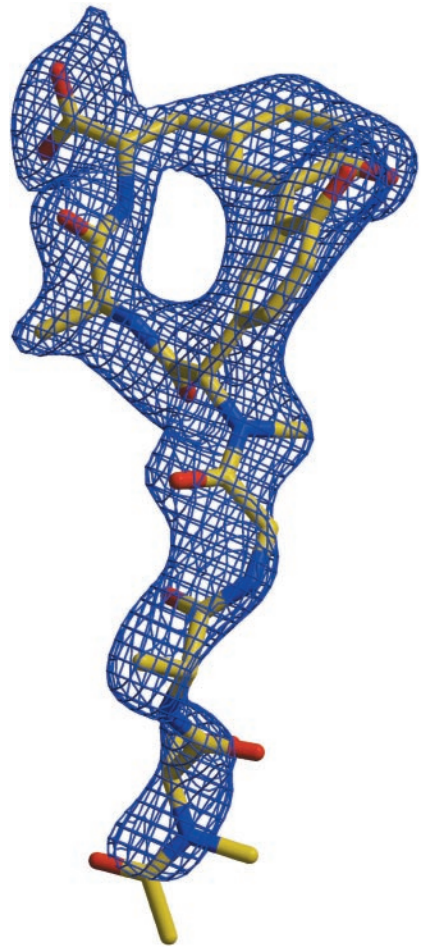

FIG. 2. **Electron density for arylomycin A_2 bound in the active site of signal peptidase.** A cross-validated $2F_o - F_c$ electron density map contoured at 1σ surrounding the signal peptidase inhibitor/antibiotic arylomycin A_2.

Isothermal Titration Calorimetry—Determination of the binding constant and full thermodynamic description of the interaction of SPase with arylomycin A_2 was achieved by isothermal titration calorimetry using a Microcal. Arylomycin A_2 was dissolved in 20 mM Tris-HCl, 5 mM $MgCl_2$, 1% Elugent™ detergent, pH 7.4, to a concentration of 450 μM and 33 separate injections were made into 1.4 ml of 15 μM SPase in the sample cell during one calorimetric run. For each run the resulting isotherm allows the number of binding sites for the ligand on each molecule, the binding association constant, and the change in reaction enthalpy upon binding to be calculated.

RESULTS

A New Crystal Form of the Catalytic Domain of E. coli Type I Signal Peptidase

Initial attempts to soak the arylomycin A_2 into pre-formed crystals of Δ2–75 were unsuccessful. Therefore new conditions were developed to co-crystallize the SPase Δ2–75 with the inhibitor. The crystals described here belong to the tetragonal crystallographic space group $P4_32_12$ and gave ordered diffraction out to 2.5 Å. This constitutes the third space group in which Δ2–75 has been crystallized and the structure solved. The acyl-enzyme inhibitor complex crystals had the orthorhombic space group $P2_12_12$ (11) and the apo-enzyme crystals had the tetragonal space group $P4_12_12$ (12). The arylomycin A_2-SPase Δ2–75 complex crystals described here form in polyethylene glycol 4000 and propanol-1, which is significantly different from the previously described crystallization conditions that used ammonium dihydrogen phosphate as the precipitant

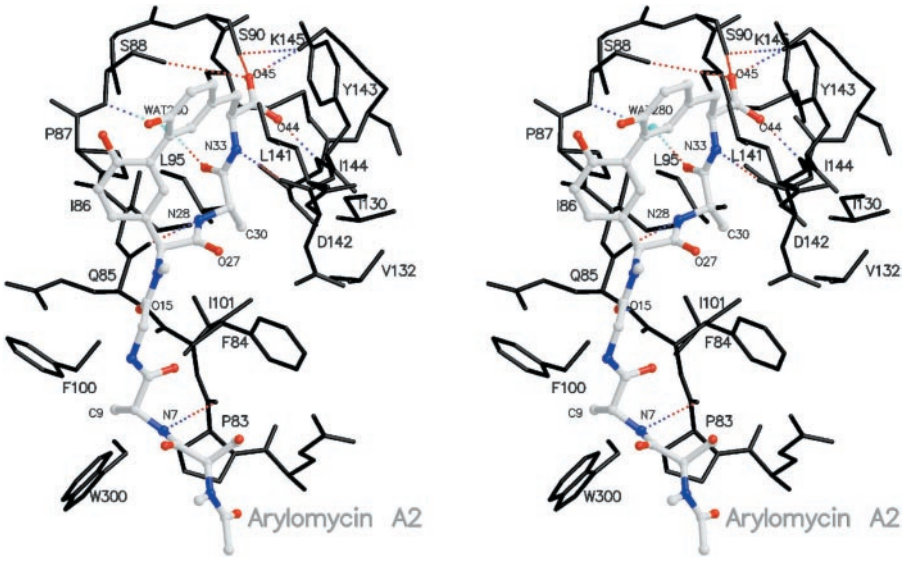

FIG. 3. **Structure of the active site of signal peptidase with a noncovalently bound biaryl-bridged lipohexapeptide inhibitor.** A stereo rendering of arylomycin A_2 bound in the active site of *E. coli* type I SPase. The protein is in *black stick* and the inhibitor is in ball-and-stick with *gray* for carbon, *blue* for nitrogen, and *red* for oxygen.

(15) (see "Experimental Procedures" for details). As with the previously described conditions, the detergent Triton X-100 was essential for crystallization. Also similar to the previous conditions, the buffer sodium citrate was used but in these new crystallization conditions the pH of the reservoir solution was pH 6.0 rather than 4.85.

Crystallographic Structure Solution of Signal Peptidase in Complex with Arylomycin A_2

A molecular replacement solution was found using the program AMORE (32). Molecule A from the previously solved 1.9-Å inhibitor acyl-enzyme crystal structure (Protein Data Bank code 1B12 (11)) was used as the search model. The program EPMR was also successful in obtaining the same solution (45). The initial $F_o - F_c$ difference map revealed a large circular density with a tail consistent with the general shape of the inhibitor. A model of the inhibitor was built, along with the topology and parameter files needed for refinement, based on the structural and stereochemical analysis of arylomycin A_2 by Höltzel *et al.* (46). Cycles of refinement and manual rebuilding of the protein model and inhibitor model using programs CNS and XFIT, respectively, were able to produce a model with a good fit to the experimental electron density (r = 23.1, R_{free} = 28.5).

Analysis of Arylomycin A_2 in the Signal Peptidase Substrate Binding Site

An average of 481 $Å^2$ of solvent accessible surface area on *E. coli* SPase is buried by arylomycin A_2 bound in the active site. The inhibitor is bound with its COOH-terminal biaryl-bridged end pointing into the active site. It binds in a parallel β-sheet fashion making interactions with both of the β-strands that line the binding site of SPase (142–145 and 83–90). The center of the biaryl-bridged ring system of the inhibitor is positioned approximately between SPase residues Pro^{87} and Leu^{141}. All of the potential main chain hydrogen bond donors and acceptors in the inhibitors 3-residue biaryl-bridged ring system (MeHpg–L-Ala–L-Tyr) are positioned to make hydrogen bonds with SPase atoms, either directly or via water molecules. In contrast, only 2 of the 6 potential main chain hydrogen bond donors or acceptor (N7 and O15) in the NH_2-terminal 3-residue tail of the inhibitor (D-MeSer–D-Ala–Gly) appear to make hydrogen bonds with SPase. Hydrogen bonding and van der Waals contacts between the lipohexapeptide inhibitor and SPase are depicted in Fig. 3 and in Table II. Interestingly, the carboxylate oxygen atom O45 of arylomycin A_2 is positioned into the SPase active site such that O45 makes hydrogen bonding interaction with each of the enzymes catalytic residues: the nucleophile Ser^{90} O-γ, the general base Lys^{145} N-ζ, and the oxyanion hole Ser^{88} O-γ. The C30 methyl group from the penultimate Ala side chain within the inhibitor points approximately into the S3 binding pocket (Table II). The C9 methyl side chain of the D-Ala residue points into a shallow pocket formed from the SPase residues Pro^{83}, Phe^{84}, Gln^{85}, Phe^{100}, and Trp^{300}. Although there is no electron density seen for the fatty acid group on the inhibitor (Fig. 2), there is electron density for the methylated D-serine at the peptide inhibitors NH_2 terminus where the fatty acid is attached. This localizes the fatty acid near the proposed SPase membrane association surface (11).

Comparison with the Acyl-enzyme and Apo-enzyme Structures of Signal Peptidase

As with the previously solved structures of Δ2–75 SPase the nucleophilic Ser^{90} O-γ and the general base Lys^{145} N-ζ are within hydrogen bonding distance (3.1 Å, an average of the 2 molecules in the asymmetric unit).

Superposition of the acyl-enzyme (Protein Data Bank code 1B12) and the apo-enzyme (1KN9) structure onto the noncovalently bound inhibitor complex structure reveals that the χ_1 angle for Ser^{88} is 74° (an average of the 2 molecules in the asymmetric unit), which is in agreement with the apo-enzyme structure and is consistent with this residue contributing a stabilizing hydrogen bond to the oxyanion carbonyl during the transition state (Fig. 4). In the acyl-enzyme structure, the Ser^{88} χ_1 was forced out of position by a clash with the thiozolidine ring of the inhibitor.

An overlap of the active sites also reveals that as a result of the hydrogen bonding interaction between the carboxylate oxygen O45 of arylomycin A_2 and the N-ζ of Lys^{145}, the χ_4 angle (−69°) of Lys^{145} is significantly different from that seen in the previous structures (168.9° for the apo-enzyme structure and 178° for the acyl-enzyme structure, averages of the 4 molecules in the asymmetric unit for each structure). The different angle for the general base lysine ϵ-amino group results in this functional group no longer making a hydrogen bond with the Ser^{278}

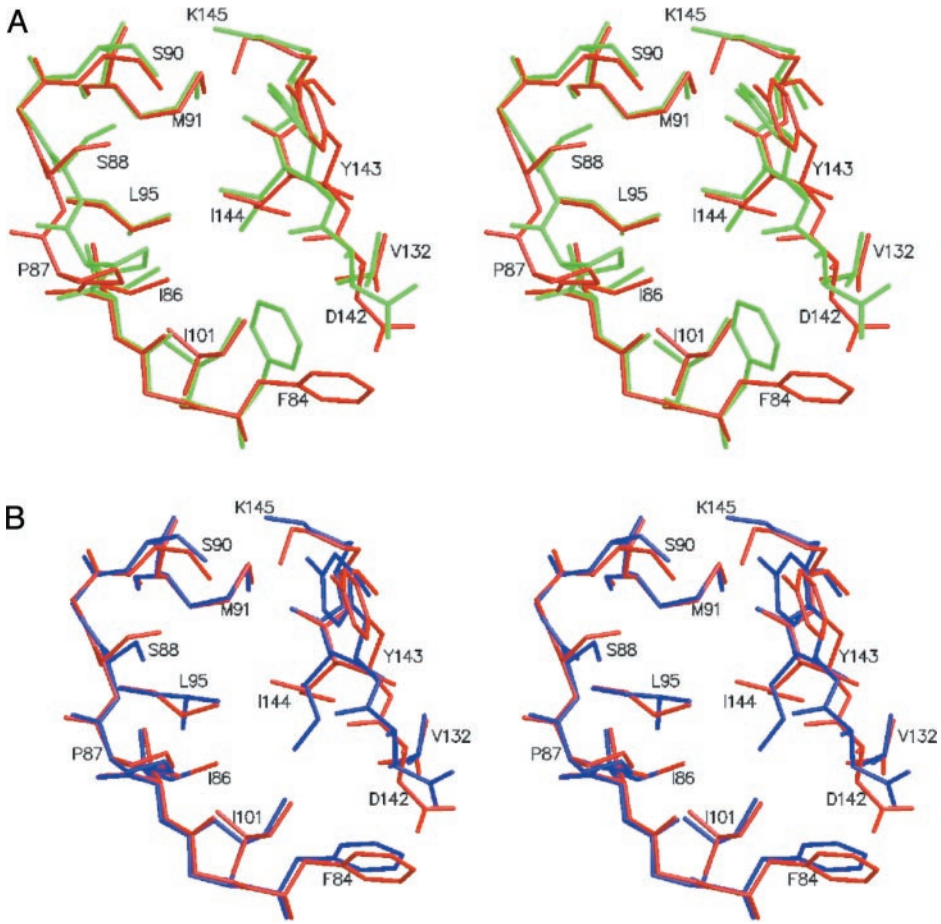

FIG. 4. **Superposition of the active site residues in the apo-enzyme, acyl-enzyme, and non-covalently bound inhibitor structures of signal peptidase.** *A*, the apo-enzyme active site residues are shown in *green* and the arylomycin A_2 bound signal peptidase active site residues are shown in *red*. *B*, the acyl-enzyme active site residues are shown in *blue* and the arylomycin A_2 bound signal peptidase active site residues are shown in *red*.

TABLE II
Inhibitor-protein contact distances

Inhibitor, atom	Protein, atom	Distance	
		Molecule A	Molecule B
		Å	
N7	Pro^{83} O	3.5	3.6
O15	Gln^{85} N	2.7	2.8
O27	Asp^{142} N (via WAT198 in molecule B)	NS[a]	3.3/2.8[b]
N28	Gln^{85} O	2.9	3.1
O32	Ser^{88} N (via WAT280 in molecule A and WAT195 in molecule B)	2.7/2.9[b]	2.7/3.0[b]
N33	Asp^{142} O	2.8	2.8
O44	Ile^{144} N/Lys^{45} N-ζ	2.6/3.2	2.6/3.0
O45	Lys^{145} N-ζ/Ser^{90} O-γ/Ser^{88} O-γ/WAT73	3.0/3.4/3.4/2.8	3.2/3.1/3.2/ NS
C30	Phe^{84} C-δ2/Asp^{142} O/Ile^{144} C-γ2, Cβ	4.1/3.8/3.8, 3.7	4.0/3.8/3.9, 3.6

[a] NS signifies that the water was not seen in the specified molecule of the asymmetric unit.
[b] Inhibitor atom to water distance / water to protein atom distance.

O-γ as seen in the previous structures. The χ_4 angle for Lys^{145} in the arylomycin A_2 bound structure is actually closer to that seen in the UmuD protein-like proteases (12, 47). The bound arylomycin A_2 almost completely buries the Lys^{145} N-ζ. The average accessible surface area for the N-ζ of Lys^{145} is 2.04 $Å^2$ with arylomycin A_2 bound, 11.49 $Å^2$ with the arylomycin A_2 removed (average of the two molecules in the asymmetric unit).

The binding pocket of this arylomycin A_2-signal peptidase complex appears to be a closer match to that of the acyl-enzyme complex structure than that of the apo-enzyme structure. For example, the phenyl ring side chain of Phe^{84} as well as the main chain near Pro^{87} are in a similar position to that seen in the penem-bound structure (Fig. 4). Molecular surface analysis of the binding pocket region (S1/S3) confirms quantitatively that the volume of the pocket (246 $Å^3$) is closer to that of the acyl-enzyme (224 $Å^3$) than that of the apo-enzyme (129 $Å^3$) (40).

Similar to both the apo-enzyme and acyl-enzyme structures, there is a buried water near Ser^{90} (WAT290 in molecule A and WAT270 in molecule B). Molecule A in the arylomycin A_2-SPase complex structure has a water (WAT289) in a similar position to that of WAT3 in the apoenzyme structure, except it is displaced by ~2 Å such that it can still coordinate with the ϵ-amino group of Lys^{145}, which, as discussed above, has a significantly different χ_4 angle from the previously solved structures because of interactions with the inhibitor. The water designated as WAT3 in the apo-enzyme structural analysis was judged to be the most likely candidate to act as the deacylating water based on its position relative to the general base lysine

and its angle of nucleophilic attack on the scissile carbonyl (Bürgi angle (48)). Arylomycin A_2 has displaced an ordered water (WAT 2 in the apoenzyme bound structure, average *B* factor = 37.78) that was hydrogen bonded to Ile^{144} N (average distance = 3.2 Å). This interaction has been replaced by a strong hydrogen bond (average distance = 2.6 Å) to O44 of arylomycin A_2. By comparing the apo-enzyme and the arylomycin A_2-bound structures we can see that the only interactions that are broken to form the final inhibitor-enzyme complex are the above mentioned displacement of the ordered water that interacted with Ile^{144} N and the above mentioned broken intra-molecular interactions between Ser^{278} O-γ and Lys^{145} N-ζ.

Spectroscopic Analysis to Probe the Binding Mechanism of Arylomycin A_2 to Signal Peptidase

Steady-state Fluorescence Spectroscopy—Binding of arylomycin A_2 in the active site of SPase causes a change in the quantum yield of fluorescence emission at 417 nm upon excitation at 280 nm. This is caused most likely by the transfer of energy from tryptophan residue(s) in or around the active site of the SPase enzyme to the arylomycin A_2 molecule. The x-ray structure of the SPase-arylomycin A_2 complex shows that the ring of the cross-linked Tyr-Hpg moiety, when bound, lies flat against a large hydrophobic surface on one side of the SPase binding site and this too could have a contributing effect to an increase in fluorescence by reducing the quenching of the arylomycin A_2 molecule. The change in fluorescence associated with the binding of arylomycin A_2 to SPase as a function of the log of ligand concentration describes a sigmoidal binding curve, from which a value of $0.94 \pm 0.04 \times 10^{-6}$ M for the binding dissociation constant (K_d) was calculated (Fig. 5). This was close to the value of $0.61 \pm 0.03 \times 10^{-6}$ M for the binding dissociation constant calculated from the reciprocal of the binding association constant determined by isothermal titration calorimetry (see below). The similarity of these two values and the fact that the fluorescence change reaches saturation at high inhibitor concentrations, as well as the goodness of fit of the isothermal titration calorimetry data to a curve describing a single binding site, demonstrates that the binding of arylomycin A_2 to SPase was specific to a single binding site and that fluorescence spectroscopy can be used to directly observe binding.

Stopped-flow Fluorescence Spectroscopy—The mode of binding of arylomycin A_2 was investigated by stopped-flow fluorescence spectroscopy. The data obtained were fitted to Equation 1 and the results are shown in Tables III and IV. The fit of all the data was demonstrated by *F*-test to be statistically much better to a double exponential curve than to a single exponential and this was the case for both fluorescence and anisotropy data (Fig. 6). Also similar trends in the rate constants were observed in both the fluorescence and anisotropy data. Because, both the fluorescence measurements and the anisotropy measurements reveal the occurrence of two exponential processes the observed rate constants can be assumed to be associated with the binding of arylomycin A_2 to SPase and the nature of the two processes involved is hypothesized as the initial contact between the ligand and the enzyme followed by a slow rearrangement. This can be described by a reaction scheme of the type,

$$E + S \underset{k_{off}}{\overset{k_{on}[S]}{\rightleftharpoons}} ES \overset{slow}{\rightleftharpoons} ES^* \qquad \text{(Eq. 3)}$$

where the enzyme and substrate first combine to form an initial collisional complex (*E*S), followed by a slow isomerism to the final bound state (*E*S*).

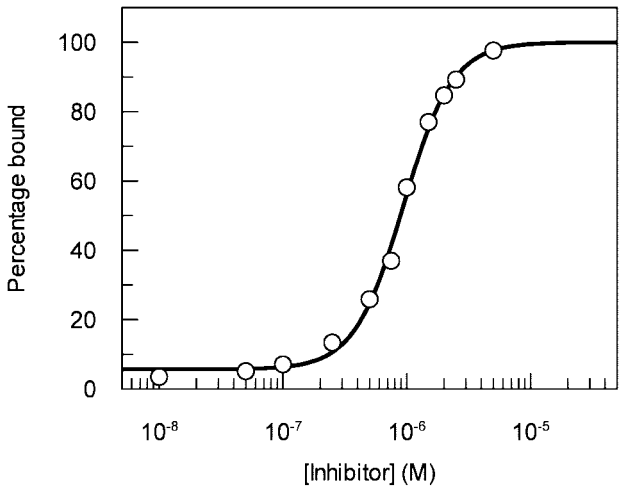

FIG. 5. **Binding of arylomycin A_2 to signal peptidase measured by steady-state fluorescence spectroscopy.** The apparent K_d value was calculated to be $0.94 \pm 0.04 \times 10^{-6}$ M.

When the concentration of ligand was in excess of SPase the amplitude of the faster of these rate constants becomes dominant, such that the amplitude of the slower rate constant is insignificant in comparison to the error in the fit of the curve. This causes a large underestimation of the slower rate constant upon fitting data obtained at high concentrations of substrate to Equation 1. However, it is clearly observable from the data in Tables III and IV that when the concentration of substrate moves from [S]<[*E*] to [S]>[*E*], the rate of the slower rate constant begins to increase until such a point as the fit becomes dominated by the faster rate constant.

The observed binding data obtained by stopped-flow fluorescence spectroscopy determined in the presence of excess substrate was fitted to Equation 1 and the faster rate constant with the greater amplitude was plotted as a linear plot according to Equation 2 (Fig. 7). From this linear plot a value of $0.45 \pm 0.02 \times 10^6$ M^{-1} s^{-1} was derived for the association rate constant (k_{on}) and a value of 0.48 ± 0.46 s^{-1} for the dissociation rate constant (k_{off}). The value for the association rate constant is several orders of magnitude lower than the diffusion-controlled limit for binding. We can see from a comparison between the apo-enzyme structure and the arylomycin A_2-bound structure that the associate rate is consistent with the many contacts that are formed between arylomycin A_2 and the SPase active site (Table II and Fig. 3) and the two hydrogen-bonding interactions that are broken to form the complex (described above). However, because it was impossible to derive data for the slower rate constant for values of substrate of 25 μM and above, the values of the association and dissociation rate constants for the slower binding process could not be calculated.

When the concentration of the enzyme is in excess of ligand, both the faster and slower rate constants are independent of ligand concentration (Table III). This relationship is predicted by the rate equation,

$$k_{obs} = k_{off} + k_{on} \cdot [E] \qquad \text{(Eq. 4)}$$

where the observed rate (k_{obs}) is pseudo first-order because the concentration of the enzyme is effectively unchanged during the reaction.

Binding Parameters Derived by Calorimetry

Differential Scanning Calorimetry—The stabilizing effect of contacts formed upon binding was investigated by measuring the melting transition (T_m) of SPase using differential scanning calorimetry. The melting transition of SPase with and

TABLE III
Kinetic rate constants obtained by stopped-flow fluorescence spectroscopy under conditions of [E] > [S], where [E] is kept at a constant concentration of 6.25 μM

Concentration of arylomycin A_2	ΔF_1	k_1	ΔF_2	k_2	Probability[a]
μM	*arbitrary units*	s^{-1}	*arbitrary units*	s^{-1}	
0.05	3.93 ± 0.03	4.58 ± 0.09	0.64 ± 0.02	0.14 ± 0.01	1.69×10^{-128}
0.25	11.78 ± 0.03	4.42 ± 0.03	2.21 ± 0.02	0.14 ± 0.01	1.96×10^{-323}
0.5	23.78 ± 0.04	4.51 ± 0.02	4.45 ± 0.03	0.14 ± 0.01	NF[b]
1.25	27.16 ± 0.03	4.46 ± 0.01	5.27 ± 0.02	0.13 ± 0.01	NF
2.5	48.09 ± 0.06	4.22 ± 0.01	9.67 ± 0.04	0.13 ± 0.01	NF
3.75	68.84 ± 0.11	4.01 ± 0.01	14.15 ± 0.07	0.14 ± 0.01	NF
5	88.45 ± 0.19	3.86 ± 0.02	18.93 ± 0.17	0.16 ± 0.01	NF

[a] Probability that a single exponential fits the data better than a two-exponential fit as determined by F-test.
[b] NF, no fit could be obtained by a single exponential.

TABLE IV
Kinetic rate constants obtained by stopped-flow fluorescence spectroscopy under conditions of [E] < [S], where [E] is kept at a constant concentration of 6.25 μM

Concentration of arylomycin A_2	ΔF_1	k_1	ΔF_2	k_2	Probability[a]
μM	*arbitrary units*	s^{-1}	*arbitrary units*	s^{-1}	
7.5	114.85 ± 0.37	3.88 ± 0.03	23.48 ± 0.31	0.23 ± 0.01	1.83×10^{-313}
10	128.67 ± 0.58	4.80 ± 0.04	25.91 ± 0.60	0.55 ± 0.02	8.03×10^{-241}
12.5	138.21 ± 0.82	6.66 ± 0.06	24.75 ± 0.91	1.16 ± 0.04	2.59×10^{-199}
25	151.86 ± 0.40	10.95 ± 0.04	4.66 ± 0.09	0.16 ± 0.01	3.10×10^{-228}
37.5	151.43 ± 0.41	18.15 ± 0.06	4.36 ± 0.07	0.13 ± 0.01	2.22×10^{-229}
50	142.20 ± 0.01	22.90 ± 0.01	3.00 ± 0.01	0.24 ± 0.01	4.74×10^{-214}

[a] Probability that a single exponential fits the data better than a two-exponential fit as determined by F-test.

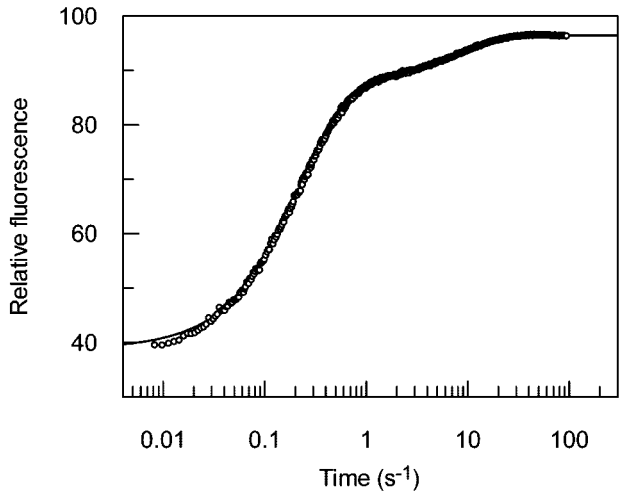

FIG. 6. **Binding curve of arylomycin A_2 binding to signal peptidase measured by stopped-flow fluorescence.** The concentration of substrate was 2.5 μM and the enzyme concentration was 6.25 μM in 20 mM Tris-HCl, 5 mM $MgCl_2$, 1% Elugent™ detergent, pH 7.4, at 25 °C. The *solid line* shows a fit to Equation 1, where k_1 is 4.2 s^{-1} and k_2 is 0.13 s^{-1}.

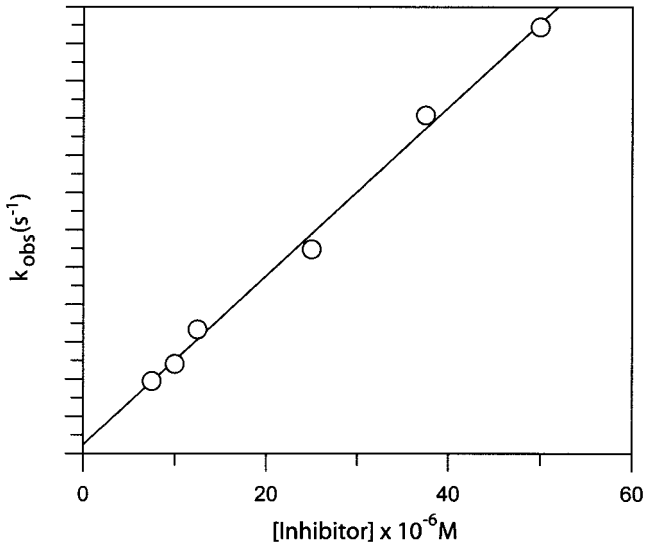

FIG. 7. **A plot of the observed binding rate constant against arylomycin A_2 concentration.** Data were plotted according to Equation 1 from which a rate constant for the association of ligand (k_{on}) of 0.45 ± 0.02 × 10^6 M^{-1} s^{-1} and a value for the rate constant for dissociation (k_{off}) of 0.48 ± 0.46 s^{-1} was obtained.

without the addition of ligand was irreversible, indicating that the system cannot be treated as being purely under thermodynamic control. However, the melting curve could still be described by a simple two-state model indicating that the enzyme unfolded as a single domain essentially free from impurities or aggregated protein prior to the increase in temperature. There was a clear increase in the T_m from 46.7 to 48.5 °C for SPase upon binding arylomycin A_2 (Fig. 8). This increase in T_m of 1.8 °C was significant in comparison to the error associated with the technique of ±0.3 °C and was most likely caused by the formation of stabilizing interactions between ligand and the SPase enzyme upon binding (Table II and Fig. 3).

Isothermal Titration Calorimetry—The binding isotherm generated by isothermal titration calorimetry was accurately fitted by a model for binding to one single binding site and gave a stoichiometry of binding of 0.95 mol of arylomycin A_2/mol of SPase, a ΔH_{cal} of −7520 cal mol^{-1} and a K_{eq} (association constant) of 1.65 ± 0.1 × 10^6 M^{-1} (Fig. 9). Because this value for K_{eq} was obtained using the same buffer conditions and at the same temperature as the stopped-flow fluorescence measurements, a value for the dissociation rate constant of 0.27 s^{-1} can be derived from the association rate constant calculated from the stopped-flow fluorescence measurements and the binding association constant obtained by isothermal titration calorimetry. This value is close to the k_{off} value calculated directly by stopped-flow fluorescence of 0.48 s^{-1} and gives much greater confidence in this value in view of the very high standard error on the measurement.

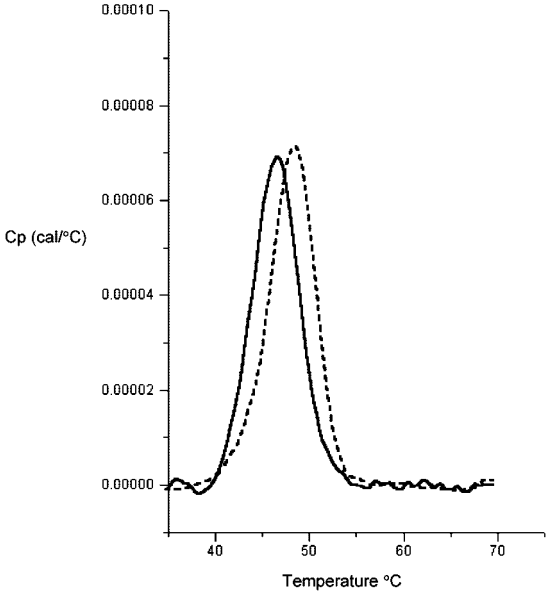

FIG. 8. **Thermograms showing the thermal unfolding of signal peptidase.** Thermal unfolding of 12.5 mg/ml signal peptidase (*solid line*) and 12.5 mg/ml signal peptidase with 100 μM arylomycin A_2 (*dashed line*) both in 20 mM Hepes, pH 8.0, with 2% Elugent™ detergent.

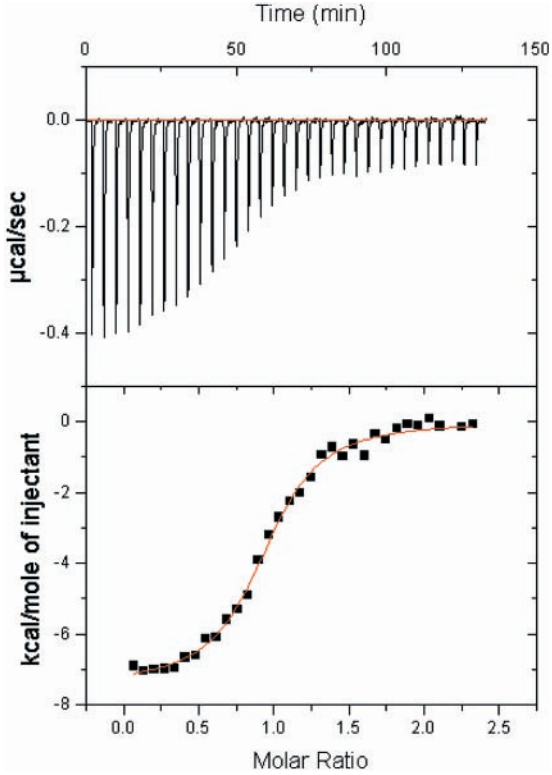

FIG. 9. **An example of the raw data (*top*) and binding isotherm (*bottom*) obtained by isothermal titration calorimetry of signal peptidase.** The concentration of signal peptidase in the sample cell was 15 μM in 20 mM Tris-HCl, 5 mM $MgCl_2$, 1% Elugent™ detergent, pH 7.4, 33 aliquots of 2.997 μl volume of 450 μM arylomycin A_2 were injected into the sample.

DISCUSSION

Here we have analyzed the structure and binding mode of the peptide-based signal peptidase inhibitor/antibiotic arylomycin A_2. This colorless natural product isolated from *Streptomyces* extracts is classified as a secondary metabolite formed by non-ribosomal peptide synthesis (49, 50). Arylomycin A_2 is one of a number of similar compounds differing in the type of fatty acid attached to the NH_2 terminus. There are actually two series of arylomycin compounds isolated and characterized (29, 46). The arylomycin B series differs from the arylomycin A series in that the B series is yellow in color resulting from the substitution of the tyrosine residue by a 3-nitrotyrosine residue. These arylomycin compounds have demonstrated antibiotic activity (29). Exchange peaks in the ROESY and NOESY spectra show that there is a *cis-trans* isomerization of the fatty acid-MeSer amide bond with the predominate geometry being *trans* (46). This isomerization may have attributed to the lack of electron density for the fatty acid (Fig. 2).

Although arylomycin A_2 is a novel biaryl-bridged lipohexapeptide, some of the structural aspects of this compound have been seen before. The Hpg residue (4-hydroxyphenylglycine) has been seen before in peptide-based antibiotics. The peptide antibiotic ramoplanin contains a Hpg residue and its structure has been solved by NMR (51) (Protein Data Bank code 1DSR). The biosynthetic pathway for 4-hydroxyphenylglycine has recently been determined (50). As mentioned above the Hpg residue in arylomycin A_2 is cross-linked via its phenol ring ortho-carbon to the phenol ring ortho-carbon of the Tyr residue. Dityrosine cross-links are occasionally seen in proteins and can be formed photochemically or enzymatically (52). The glycopeptide antibiotic vancomycin has a 3-residue ring system similar to arylomycin A_2 including the Hpg-Tyr cross-link. The crystal structure of vancomycin alone has been solved at atomic resolution (Protein Data Bank codes 1SHO (53) and 1AA5 (54)). Its structure has also been solved in complex with the cell wall precursor analog, di-acetyl-Lys-D-Ala-D-Ala (Protein Data Bank code 1FVM).

There is a large amount of literature supporting the idea that cyclization of peptides (macrocyclization) can cause a significant reduction in the conformational freedom that often results in increased receptor binding affinity (55). Although it is possible that the biaryl-bridge in arylomycin A_2 could increase the rigidity and limit the conformational freedom of arylomycin A_2 such that fewer non-productive conformations would have to be sampled during the binding event with signal peptidase, this has proven to be difficult to test with the comparable linear peptide. Unfortunately, linear peptides based around arylomycin A_2 or substrate consensus sequences do not bind sufficiently tightly to measure the thermodynamic parameters. The entropy change (ΔS) from our isothermal titration calorimetry analysis of arylomycin A_2 binding to SPase is 11 J/mol, therefore the major thermodynamic factor is the reaction enthalpy presumably driven by hydrogen bonding interactions between the inhibitor and the signal peptidase binding site.

It is possible that the NH_2-terminal fatty acid chain of arylomycin A_2 contributes to the effectiveness of the inhibitor by presenting the correct orientation of the inhibitor to the SPase binding site within the lipid bilayer *in vivo* or in the detergent micelle in *in vitro* assays. Peptide substrates designed for signal peptidase with NH_2-terminal fatty acid tails show significantly more activity than that of similar peptides without fatty acids (56). Although we do not see electron density for the fatty acid in this structure we do see density for the NH_2 terminus of the lipopeptide inhibitor where the fatty acid is attached (Fig. 2). The NH_2 terminus of arylomycin A_2 is located adjacent to Trp^{300}, which is part of the proposed SPase membrane association surface (Fig. 3). Interestingly, Trp^{300} has been shown by chemical modification and mutagenesis to be an important residue for SPase activity (57).

Both the crystallographic analysis and the spectroscopic data are consistent with arylomycin A_2 binding specifically to a single binding site on SPase. The fluorescence data is most consistent with a two-step binding mechanism. This mecha-

nism involves a rapid binding mode followed by a slow isomerism to the final bound state and these two separate binding events were readily identified by stopped-flow fluorescence because the isomerism step has a much lower rate than the formation of the initial collisional complex. A comparison of the active site regions of the apo-enzyme, acyl-enzyme, and the noncovalently bound complex with arylomycin A_2 (Fig. 4) shows that the proposed slow isomerization step of the two-state process of binding is unlikely to be the result of the need for large structural adjustments in SPase. The observed net effect on the SPase active site region upon binding of ligands is a change in the volume of the specificity subsites that is a result of a rotation in the side chain position of Phe^{84} and some main chain movement near Pro^{87}. Future NMR analysis of the structure and dynamics of arylomycin A_2 in solution may help provide insights into whether the slow isomerization step may be because of structural adjustments needed in the arylomycin A_2 molecule before the correct docking mode is established in the active site of SPase.

The relatively low value for the binding association rate constant of $0.45 \pm 0.02 \times 10^6$ M^{-1} s^{-1}, in comparison to the diffusion controlled limit, demonstrates the breaking and formation of interactions during binding is in agreement with the stabilization of the melting temperature measured by DSC. These biophysical results are consistent with the crystallographic analysis that revealed that the final arylomycin A_2 bound form of the enzyme requires the formation of many new intermolecular interactions between the enzyme and arylomycin A_2 (Table II and Fig. 3). Interestingly, the formation of the final complex requires the breaking of only one intra-molecular hydrogen bond (Ser^{278} O-γ to Lys^{145} N-ζ) and the displacing of one water that was observed in the binding site in the apo structure (WAT2 (12)). Further experiments will need to be performed to analyze the temperature dependence and activation energies of the individual binding steps to make a connection between the slow binding association rate and the thermodynamic stabilization of the final inhibitor-enzyme complex.

The observed interactions between this non-covalently bound hexapeptide inhibitor and SPase agree very well with the previously proposed model of a signal peptide bound in the active site of *E. coli* signal peptidase (12), which was based on the crystal structure of the LexA cleavage site (58). Both the model and the inhibitor complex show hydrogen-bonding interactions with both the main chain carbonyl and amide of Gln^{85}. Because the COOH-terminal carboxyl group of the inhibitor sits approximately where the P1 residue of the pre-protein substrate would reside, the interactions with the strand containing the general base lysine are not quite the same. The L-Ala methyl side chain (C30) of arylomycin A_2 sits in the shallow hydrophic pocket, which was proposed previously from modeling studies to be the S3 binding pocket. The D-Ala methyl side chain (C9) of arylomycin A_2 points into a shallow pocket that possibly could be the S5 binding pocket. The overall path traced out by the inhibitor suggests that pre-proteins may interact more with the residues that make up the N-terminal β-strand (83–90) than the residues that make up the strand containing the general base (142–145). It is presumed from the primary sequence analysis of signal peptides and the thickness of the lipid bilayer that residues after the P6 residue, namely P7 and the other residues forming the hydrophobic core of the signal peptide would form a helical structure and not be available for main chain interactions with SPase. Future crystal structures of mutant enzyme with peptide substrates will help to clarify and confirm the enzyme-substrate contacts.

Acknowledgments—We thank Dr. Robert Sweet at the Brookhaven National Laboratory NSLS beam line X8C. We thank Dr. Natalie C. J. Strynadka, Denise Dombroski, Dr. Yu Luo, and Daniel Lim for help in data collection and crystallization.

REFERENCES

1. Paetzel, M., Dalbey, R. E., and Strynadka, N. C. (2000) *Pharmacol. Ther.* **87,** 27–49
2. Carlos, J. L., Paetzel, M., Klenotic, P. A., Strynadka, N. C., and Dalbey, R. E. (2001) *The Enzymes* **22,** 27–55
3. Paetzel, M., Karla, A., Strynadka, N. C., and Dalbey, R. E. (2002) *Chem. Rev.* **102,** 4549–4580
4. Barrett, A. J., and Rawlings, N. D. (1995) *Arch. Biochem. Biophys.* **318,** 247–250
5. Date, T., and Wickner, W. (1981) *Proc. Natl. Acad. Sci. U. S. A.* **78,** 6106–6110
6. Wolfe, P. B., Wickner, W., and Goodman, J. M. (1983) *J. Biol. Chem.* **258,** 12073–12080
7. Dalbey, R. E., and Wickner, W. (1985) *J. Biol. Chem.* **260,** 15925–15931
8. Wolfe, P. B., Silver, P., and Wickner, W. (1982) *J. Biol. Chem.* **257,** 7898–7902
9. Tschantz, W. R., and Dalbey, R. E. (1994) *Methods Enzymol.* **244,** 285–301
10. Tschantz, W. R., Sung, M., Delgado-Partin, V. M., and Dalbey, R. E. (1993) *J. Biol. Chem.* **268,** 27349–27354
11. Paetzel, M., Dalbey, R. E., and Strynadka, N. C. (1998) *Nature* **396,** 186–190
12. Paetzel, M., Dalbey, R. E., and Strynadka, N. C. (2002) *J. Biol. Chem.* **277,** 9512–9519
13. Kuo, D. W., Chan, H. K., Wilson, C. J., Griffin, P. R., Williams, H., and Knight, W. B. (1993) *Arch. Biochem. Biophys.* **303,** 274–280
14. Tschantz, W. R., Paetzel, M., Cao, G., Suciu, D., Inouye, M., and Dalbey, R. E. (1995) *Biochemistry* **34,** 3935–3941
15. Paetzel, M., Chernaia, M., Strynadka, N., Tschantz, W., Cao, G., Dalbey, R. E., and James, M. N. (1995) *Proteins* **23,** 122–125
16. Paetzel, M., and Strynadka, N. C. (1999) *Protein Sci.* **8,** 2533–2536
17. Sung, M., and Dalbey, R. E. (1992) *J. Biol. Chem.* **267,** 13154–13159
18. Paetzel, M., Strynadka, N. C., Tschantz, W. R., Casareno, R., Bullinger, P. R., and Dalbey, R. E. (1997) *J. Biol. Chem.* **272,** 9994–10003
19. Carlos, J. L., Klenotic, P. A., Paetzel, M., Strynadka, N. C., and Dalbey, R. E. (2000) *Biochemistry* **39,** 7276–7283
20. Bullock, T. L., Breddam, K., and Remington, S. J. (1996) *J. Mol. Biol.* **255,** 714–725
21. James, M. N. (1994) in *Proteolysis and Protein Turnover* (Bond, J. S., and Barrett, A. J., eds) pp. 1–8, Portland, Brookfield, VT
22. Black, M. T., Munn, J. G., and Allsop, A. E. (1992) *Biochem. J.* **282,** 539–543
23. Zwizinski, C., Date, T., and Wickner, W. (1981) *J. Biol. Chem.* **256,** 3593–3597
24. Kim, Y. T., Muramatsu, T., and Takahashi, K. (1995) *J. Biochem.* (*Tokyo*) **117,** 535–544
25. Kuo, D., Weidner, J., Griffin, P., Shah, S. K., and Knight, W. B. (1994) *Biochemistry* **33,** 8347–8354
26. Black, M. T., and Bruton, G. (1998) *Curr. Pharm. Des.* **4,** 133–154
27. Wickner, W., Moore, K., Dibb, N., Geissert, D., and Rice, M. (1987) *J. Bacteriol.* **169,** 3821–3822
28. Barkocy-Gallagher, G. A., and Bassford, P. J., Jr. (1992) *J. Biol. Chem.* **267,** 1231–1238
29. Schimana, J., Gebhardt, K., Holtzel, A., Schmid, D. G., Sussmuth, R., Muller, J., Pukall, R., and Fiedler, H. P. (2002) *J. Antibiot.* (*Tokyo*) **55,** 565–570
30. Matthews, B. W. (1968) *J. Mol. Biol.* **33,** 491–497
31. Otwinowski, Z. (1993) in *Denzo* (Sawyer, L., Isaacs, N., and Baily, S., eds) pp. 56–62, SERC Daresbury Laboratory, University of Texas Southwestern Medical Center at Dallas
32. Collaborative Computational Project Number 4 (1994) *Acta Crystallogr. D Biol. Crystallogr.* **50,** 760–763
33. McRee, D. E. (1999) *J. Struct. Biol.* **125,** 156–165
34. Brunger, A. T., Adams, P. D., Clore, G. M., DeLano, W. L., Gros, P., Grosse-Kunstleve, R. W., Jiang, J. S., Kuszewski, J., Nilges, M., Pannu, N. S., Read, R. J., Rice, L. M., Simonson, T., and Warren, G. L. (1998) *Acta Crystallogr. D Biol. Crystallogr.* **54,** 905–921
35. Kleywegt, G. J. (1995) *CCP4/ESF-EACBM Newsletter on Protein Crystallography* **31,** 45–50
36. van Aalten, D. M., Bywater, R., Findlay, J. B., Hendlich, M., Hooft, R. W., and Vriend, G. (1996) *J. Comput. Aided Mol. Des.* **10,** 255–262
37. Laskowski, R. A., MacArthur, M. W., Moss, D. S., and Thornton, J. M. (1993) *J. Appl. Crystallogr.* **26,** 283–291
38. Hutchinson, E. G., and Thornton, J. M. (1996) *Protein Sci.* **5,** 212–220
39. Jones, T. A., Zou, J.-Y., Cowan, S. W., and Kieldgaard, M. (1991) *Acta Crystallogr. A* **47,** 110–119
40. Liang, J., Edelsbrunner, H., and Woodward, C. (1998) *Protein Sci.* **7,** 1884–1897
41. Tsodikov, O. V., Record, M. T., Jr., and Sergeev, Y. V. (2002) *J. Comput. Chem.* **23,** 600–609
42. Meritt, E. A., and Bacon, D. J. (1997) *Methods Enzymol.* **277,** 505–524
43. Kraulis, P. G. (1991) *J. Appl. Crystallogr.* **24,** 946–950
44. Berman, H. M., Westbrook, J., Feng, Z., Gilliland, G., Bhat, T. N., Weissig, H., Shindyalov, I. N., and Bourne, P. E. (2000) *Nucleic Acids Res.* **28,** 235–242
45. Kissinger, C. R., Gehlhaar, D. K., and Fogel, D. B. (1999) *Acta Crystallogr. D Biol. Crystallogr.* **55,** 484–491
46. Holtzel, A., Schmid, D. G., Nicholson, G. J., Stevanovic, S., Schimana, J., Gebhardt, K., Fiedler, H. P., and Jung, G. (2002) *J. Antibiot.* (*Tokyo*) **55,** 571–577
47. Peat, T. S., Frank, E. G., McDonald, J. P., Levine, A. S., Woodgate, R., and Hendrickson, W. A. (1996) *Nature* **380,** 727–730
48. Burgi, H. B., Dunitz, J. D., and Shefter, E. (1973) *J. Am. Chem. Soc.* **95,** 5065–5067
49. Cane, D. E., Walsh, C. T., and Khosla, C. (1998) *Science* **282,** 63–68
50. Hubbard, B. K., Thomas, M. G., and Walsh, C. T. (2000) *Chem. Biol.* **7,** 931–942
51. Kurz, M., and Guba, W. (1996) *Biochemistry* **35,** 12570–12575
52. Kanwar, R., and Balasubramanian, D. (2000) *Biochemistry* **39,** 14976–14983

53. Schafer, M., Schneider, T. R., and Sheldrick, G. M. (1996) *Structure* **4,** 1509–1515
54. Loll, P. J., Bevivino, A. E., Korty, B. D., and Axelsen, P. H. (1997) *J. Am. Chem. Soc.* **119,** 1516
55. Davies, J. S. (2003) *J. Pept. Sci.* **9,** 471–501
56. Bruton, G., Huxley, A., O'Hanlon, P., Orlek, B., Eggleston, D., Humphries, J., Readshaw, S., West, A., Ashman, S., Brown, M., Moore, K., Pope, A., O'Dwyer, K., and Wang, L. (2003) *Eur. J. Med. Chem.* **38,** 351–356
57. Kim, Y. T., Muramatsu, T., and Takahashi, K. (1995) *Eur. J. Biochem.* **234,** 358–362
58. Luo, Y., Pfuetzner, R. A., Mosimann, S., Paetzel, M., Frey, E. A., Cherney, M., Kim, B., Little, J. W., and Strynadka, N. C. (2001) *Cell* **106,** 1–10